

Microscopic and macroscopic analysis of granular material behaviour in 3d flat-bottomed hopper by the discrete element method

R. BALEVIČIUS¹⁾, R. KAČIANAUSKAS²⁾, Z. MRÓZ³⁾,
I. SIELAMOWICZ⁴⁾

¹⁾*Dept. of Reinforced Concrete and Masonry Structures
Vilnius Gediminas Technical University
Sauletekio al. 11, Vilnius, Lithuania*

²⁾*Laboratory of Numerical Modelling
Vilnius Gediminas Technical University
Sauletekio al. 11, Vilnius, Lithuania*

³⁾*Institute of Fundamental Technological Research
Polish Academy of Sciences
Świętokrzyska 21, Warsaw, Poland*

⁴⁾*Chair of Structural Mechanics, Civil Engineering Department
Białystok Technical University
Wiejska 45E, Białystok, Poland*

THE PAPER PRESENTS the application of the discrete element method to modelling of granular material filling and discharge in 3D flat-bottomed hopper. A mathematical model, as well as the developed software code, operates with spherical visco-elastic non-cohesive frictional particles. The evolution of granular flow, internal forces and densification (rarefaction) are characterized by macroscopic parameters such as the discharge rates, the porosity fields and the wall pressures, as well as by microscopic evaluations in terms of coordination number, velocity patterns and inter-particle contact forces. It was shown that qualitative characterization of flow may be done even by relatively rough models with small number of particles, which required to be increased, however, for more precise description of the localized phenomena. Unsatisfactory evaluation of the stress peak during discharge is presented as an illustrative example. The main focus of the paper is the analysis of particle friction effect and the consistency of micro and macro-phenomena in the time-dependent flow process.

Key words: discrete element method, spherical particles, visco-elastic granular material, three-dimensional flat bottomed hopper.

1. Introduction

THE PHYSICS OF GRANULAR MATERIALS spans a wide variety of intriguing phenomena, the explanation of which remains still a challenge for various research

and engineering areas [1–5]. Actually, theoretical understandings about the granular phenomena are largely empirical, while the influence of microscopic granular properties and inter-granular relations on the macroscopic dynamical behaviour of the whole granular material is highly complicated.

The investigations of granular material behaviour in hoppers have become an actual problem in view of their broad engineering applications, where filling and discharge of granular material in hoppers are important industrial operations. Comprehensive historical review on the matter, along with handling technology as well as characterization procedures and designed methodologies presented from the engineering point of view, may be found in the works by ROBERTS [6, 7].

Fundamentals of analytical continuum-based modeling of granular material flowing in silo/hoppers have experienced significant theoretical development since the days of JANSSEN [8], when the best-known method of calculating wall pressure had been introduced. So far, the continuum models have been used in analyzing the stress states and deformation modes of granular materials, assuming the combined models of elastic, plastic or viscous response. A comprehensive review of experimental observations and theoretical models can be found in books by DRESCHER [9] and NEDDERMAN [10].

The analytical models for evaluation of the filling and discharge state of the elastic and elastic-plastic matter is presented by e.g., MRÓZ and SZYMAŃSKI [11], MRÓZ and SIELAMOWICZ [12]. Non-analytical density dependent continuum model termed as granular elasticity was suggested by KRIMER *et al.* [13] and extended in the later work by BRÄUER *et al.* [14] by considering stress distribution in silos under point loads. Discussions of the above mentioned Janssen's wall pressure evaluation and various modifications are given in [3, 15, 16].

The principal category within these approaches is attributed to the application of the Finite Element Method (FEM). An assessment of the state of art on the implementation of latter technique has been performed by HOLST *et al.* [17]. They have involved a large number of different research groups from different countries, each using their own programs, showing the strengths and weaknesses of the FEM in modelling the silo filling processes.

The continuum approach does not permit any behaviour occurring at the scale of individual particles. Therefore, it is difficult to establish the stress state within a granular material and changes in direction of sliding surfaces during filling and discharge, as well as to capture dynamical response of granules when transition from the unsteady to the steady flow is required. To improve the mentioned shortcomings, sophisticated models were proposed, in particular, within the elasto-plastic Cosserat type theory, TEJCHMAN and GUDEHUS [18], visco-elastic-plasticity, the non-associated viscoplasticity, ELASKAR *et al.* [19], the polar-hypoplasticity, TEJCHMAN and UMMENHOFER [20].

Recently, the discrete element method (DEM) introduced by CUNDALL and STRUCK [21] has been developed and applied in the analysis of flow of granular materials (e.g. [22, 23]). This method constitutes an useful and powerful alternative for numerical simulation of granular media. It is based on application of Newton's law specifying the dynamic equilibrium of grains with account for grain contact slip and frictional interaction. CAMPBELL and BRENNEN [24], WALTON [25], THORNTON [26] were the first to apply discrete methods to the silo flow problems. In this method, a limited number of particles was used and, in spite of this fact, THORNTON [26] obtained some interesting results concerning the flow rate and velocity profiles. However, the analyses operating with spherical particles have mainly been attributed to the several cases of granular flow in 2D plane-shaped [27, 28], or cylindrical [29] silos. Rather than apply non-spherical particles, FERELLEC *et al.* [30] used spherical particles by imposing an additional elastic spring, dashpot and a slider resisting the rotation of granules during the discharge from a flat-bottomed silo in 2D discrete particle simulation. In this way, flow patterns were investigated. The functional dependences of the orifice size on the flow discharge rates under steady state conditions in cylindrical rough-walled silo have also been studied by HIRSHFELD and RAPAPORT [31]. The discrete element method was also applied to multi-objective optimization of parameters of granular flow by specifying geometric and frictional hopper parameters [32]. Probably the most detailed study concerning transition from 2D to purely 3D particle state was considered by LANDRY *et al.* [15]. Recently, the sophisticated treatments to simulate granular flow in hoppers by using non-spherical discs and cylinders and sphero-discs have been applied by LANGSTON *et al.* [33], LI *et al.* [34]. The cohesive bonds at particle contacts were studied in some papers, cf. LESZCZYŃSKI [35, 36].

One of the most serious drawbacks of the DEM simulations may be attributed to validation of models by experiments. Lack of the predictable microscopic data of particles may be partially compensated by experimentally obtained macroscopic data. Therefore, elaboration of experimental data and calibration of numerical models appears to be a proper way in development of both the DEM and the reliable design of silos.

In the present paper, the filling and discharge processes in a 3-D flat-bottomed hopper are analyzed by applying the discrete element method. Spherical particles are applied in modelling by assuming non-cohesive frictional and viscoelastic contact interaction. The evolution of granular flow, internal forces and densification (rarefaction) are characterized by macroscopic parameters such as the discharge rates, the porosity fields and the wall pressures, as well as by microscopic evaluations in terms of the coordination number, velocity patterns and inter-particle contact forces. A qualitative characterization of the filling and discharge processes is obtained by models operating with quite small numbers of

particles. Unsatisfactory evaluation of the stress peak during discharge is presented as an illustrative example. The main focus of the paper is the analysis of particle friction effect and the consistency of micro and macro-phenomena in the time-dependent flow process.

An outline of the paper is as follows. The concept of the DEM and governing relations are briefly presented in Sec. 2. The hopper geometry, material data and description of numerical experiment are given in Sec. 3. Description of the microscopic and macroscopic analysis and discussions are presented in Sec. 4 and Sec. 5, respectively. Conclusions are drawn in Sec. 6.

2. Governing relations

The granular material is considered as N number of discrete spherical particles referred to as discrete elements with geometric representation of their surfaces and description of physical state. The composition of the media is time-dependent since individual particles undergo variation of their position due to free rigid body motion or because of contact with the neighboring particles or the walls. Accordingly, Newton's second law is applied to each particle i in order to describe its translational and rotational motion according to:

$$(2.1) \quad m_i \frac{d^2 \mathbf{x}_i}{dt^2} = \mathbf{F}_i$$

$$(2.2) \quad I_i \frac{d^2 \boldsymbol{\theta}_i}{dt^2} = \mathbf{T}_i$$

where \mathbf{x}_i , $\boldsymbol{\theta}_i$ are the vectors of the position of the center of gravity and the orientation of the particle, m_i is the mass of the particle i ($i = 1, N$), I_i is the inertia moment of the particle, t is the time.

Vectors \mathbf{F}_i and \mathbf{T}_i present the sums of the resultant contact forces \mathbf{F}_{ij} (including the gravity force) and torques \mathbf{T}_{ij} , that act on the particle i , respectively:

$$(2.3) \quad \mathbf{F}_i = \sum_{j=1, j \neq i}^N \mathbf{F}_{ij} + m_i \mathbf{g}$$

$$(2.4) \quad \mathbf{T}_i = \sum_{j=1, j \neq i}^N \mathbf{T}_{ij} = \sum_{j=1, j \neq i}^N \mathbf{d}_{cij} \times \mathbf{F}_{ij}$$

\mathbf{g} is the vector of gravity acceleration, \mathbf{d}_{cij} is the vector specifying a position of the contact point with respect to the centers of the contacting particles [37].

The mutual impact of particles is approximated by a representative overlap area of particle shapes in the vicinity of the point of contact. This allows for the application of the contact mechanics laws a single particle. Hence, the resulting

contact force \mathbf{F}_{ij} arising from a visco-elastic collision between particles i and j and acting on this point is expressed in terms of the normal and the tangential components:

$$(2.5) \quad \mathbf{F}_{ij} = \mathbf{F}_{n,ij}^e + \mathbf{F}_{n,ij}^v - \mathbf{t}_{ij} \min \left(|\mathbf{F}_{t,ij}^{st}|, |\mathbf{F}_{t,ij}^{dyn}| \right)$$

where $\mathbf{F}_{n,ij}^e$ and $\mathbf{F}_{n,ij}^v$ are the vectors of elastic and viscous damping force normal to the contact surface, $\mathbf{F}_{t,ij}^{st}$ and $\mathbf{F}_{t,ij}^{dyn}$ are the vectors of static and dynamic friction force in tangential direction to the contact surface, \mathbf{t}_{ij} is the unit vector of tangential direction following the orientation of tangential velocity $\mathbf{v}_{t,ij}$ of colliding particles i and j [37].

Normal repulsion forces between the particles i and j arising from their visco-elastic collision are expressed as follows, according to [22] and [37]:

$$(2.6) \quad \mathbf{F}_{n,ij}^e = \frac{2}{3} \cdot \frac{E}{(1-\nu^2)} R_{ij} h_{ij} \mathbf{n}_{ij}$$

$$(2.7) \quad \mathbf{F}_{n,ij}^v = -\gamma_n m_{ij} \mathbf{v}_{n,ij}$$

where E and ν are the elastic modulus and Poisson's ratio of the particle material, h_{ij} is the overlap between two contacting particles [37], R_{ij} and m_{ij} are the reduced radius and reduced mass of two contacting particles i and j [37], \mathbf{n}_{ij} is the unit vector normal to the contact surface and directed towards the particle i [37], $\mathbf{v}_{n,ij} = (\mathbf{v}_{ij} \cdot \mathbf{n}_{ij}) \mathbf{n}_{ij}$ is the normal component of relative contact velocity, where \mathbf{v}_{ij} is relative velocity of particles at the contact point [37]; γ_n is a viscous damping coefficient in normal direction.

The formulation of a model for the tangential force is more complicated, since the phenomena of tangential deformation and friction have to be modeled, whereas in general, they depend on the normal force $\mathbf{F}_{n,ij}$ and depth of overlap h_{ij} , as well as on the history of the tangential slip vector $\delta_{t,ij}$. The friction force describes the friction prior to a gross sliding, while the dynamic friction force delineates the friction after a gross sliding. The most general form of the static friction was proposed by KOHRING [38] in terms of simplified expressions of MINDLIN'S theory [39]:

$$(2.8) \quad \mathbf{F}_{t,ij}^{st} = -\frac{8}{3} \cdot \frac{G \sqrt{R_{ij} h_{ij}}}{(2-\nu)} \boldsymbol{\delta}_{t,ij} - \gamma_t m_{ij} \mathbf{v}_{t,ij}$$

where $\boldsymbol{\delta}_{t,ij} = \int \mathbf{v}_{t,ij}(t) dt$, G is shear modulus of the particle material, γ_t is viscous damping coefficient in tangential direction.

The dynamic friction force is expressed by Coulomb's law:

$$(2.9) \quad \mathbf{F}_{t,ij}^{dyn} = -\mu |\mathbf{F}_{n,ij}^e + \mathbf{F}_{n,ij}^v| \mathbf{t}_{ij}$$

where μ is the particle friction coefficient.

The numerical solutions of differential Eqs. (2.1)–(2.2) for each particle i at the time $t + \Delta t$ (where Δt is the time step) is performed by using the 5-th – order *Gear’s predictor-corrector* [40] scheme. A detailed description of DEM technique used in the present investigation can also be found in [41] and [42].

In general, formulation of DEM model comprises not only formulation of the equations of motion (2.1)–(2.2) with respect to (2.3)–(2.9) but also the boundary conditions. The boundary conditions represent a unilateral constraint restricting the motion of particles outward to the computational domain. It is convenient to implement the geometry of the boundary plane surface by using the equations of infinite planes [37]. However, this approach is useful when the configuration of computational domain is of a relatively simple, continuous shape and does not require the inward/outward contact detection between the particle and the boundary plane. To create the computational domain reflecting the configuration of 3D hoppers having, for example, the bottom with the orifice, the planes of a finite size have to be implemented. Such planes form the shape of a hopper, controlling the granular material flow inside the hopper (in the case of filling) and outside the hopper (in the case of discharge). The geometry of each boundary surface is sketched in the global coordinates system by using three plane corner vectors, whilst the constraints as well as particle-wall overlapping are checked in the local coordinate frame. The hopper walls (including the bottom) are assumed to be rigid and are considered as the fixed boundaries possessing friction.

3. Numerical experiment

The geometry of flat-bottomed hopper is depicted in Fig. 1. The characteristic dimension of the outlet D is assumed to be related to the average diameter d of the particle as $D = 10 d$. The thickness of the hopper at the bottom is assumed to be $b = 5 d$. The dimension of the top hopper edge is $L = 2.33 D$, while the overall height of the hopper is $H = 3.33 D$. Assuming that $d = 0.06$ m, the main geometrical parameters of the hoppers are defined as: $b = 0.3$ m, $H = 2.0$ m, $L = 1.4$ m, $D = 0.6$ m.

The granular matter is represented as an assembly of $N = 1,980$ close-size distributed particles. The values of the particle radii R_i varying over the range of 0.03 and 0.035 m are generated assuming a uniform diameter distribution. The particle physical data for the assumed visco-elastic material are given in Table 1. The assumed value of the normal viscous damping coefficient constitutes about 10% of the critical damping coefficient in collision of two particles. Inter-particle and particle-wall friction is specified by the same friction coefficient μ , indicating the case of fully rough walls.

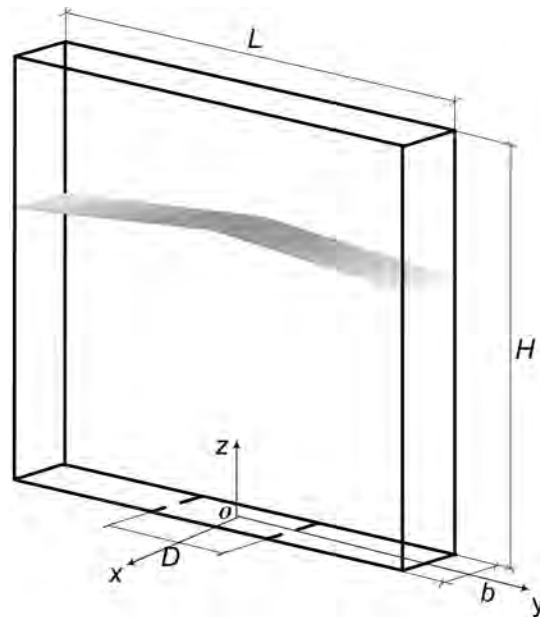


FIG. 1. The geometry of the pyramidal hopper.

Table 1. Basic data on granular material.

| Quantity | Symbol | Value |
|---|------------|-------------------|
| Density, kg/m^3 | ρ | 500 |
| Poisson's ratio | ν | 0.30 |
| Elasticity modulus, Pa | E | $0.3 \cdot 10^6$ |
| Shear modulus, Pa | G | $0.11 \cdot 10^6$ |
| Normal viscous damping coefficient, 1/s | γ_n | 60.0 |
| Tangential viscous damping coefficient, 1/s | γ_t | 10.0 |

In general, filling comprises the settling of the material into the hopper. The discharge means a flow of material from the hopper due to the orifice opening. Processes of the filling and discharge can be performed by different simulation scenarios which can affect the stress transmission within granular matter, as well as the geometry of granular structure. The choice of simulation scenario must highlight an attempt to achieve as close as possible, the situation encountered in real hoppers, as well as to save the computation time needed.

To obtain the compromise between these requirements, the filling is simulated by sedimentation of particles *en masse*, i.e. all particles start to fall due to gravity acceleration and to mix up when the initial particle velocities are also artificially imposed. During the particles settling on the bottom in the filling process, the orifice is kept closed until a quasi-static state occurs. The discharge process

begins after an instant opening of the orifice. During the discharge no material re-supply from above is made.

By following the above scenario, the initial state for commencing of the filling is generated in the following manner. The space within and above the hopper was divided into the cubic cells as an orthogonal and uniform 3D grid of 0.1 m. Initially, at time $t = 0$, the particles are embedded free of contact into the centers of these cells. The fields of initial velocities are defined randomly with uniform distribution, to have their magnitude varying in the range from 0 to 0.3 m/s.

The behaviour of a granular material during filling was controlled by the evolution of the total kinetic energy of granular material, expressed as the sum of all particle energies due to translational and rotational motion. The evolution of the kinetic energy to zero value is assumed to be a stabilization indicator of the filling process of granular material, allowing *de facto* to interrupt the simulation.

The time-evolution of kinetic energy reflects a sophisticated integral behavior of the flow. Generally, frictional particles lose energy not only due to material viscous damping but additionally due to friction. In this case, the particles start to rotate, affecting the translational motion. The effect of friction is manifested throughout the competition between static and dynamic friction forces. This competition leads to significant fluctuation of relative inter-particle contact velocities $\mathbf{v}_{t,ij}$, particle velocities \mathbf{v}_i and, in turn, the evolution of the total kinetic energy. Frictionless material is subjected, however, to a higher fluctuation since particles are able to dissipate the kinetic energy only due to the damping in the normal direction. Stabilization of the total kinetic energy means that most of the particles have dropped on the bottom and cannot essentially change the positions relatively to their neighbours.

Stabilization of the granular flow is a rather hypothetical state which may be achieved within the limits of the required tolerance. On the basis of computational experience, the state of rest is indicated by the level of total kinetic energy equal to $0.3 \cdot 10^{-6}$ J which specifies the average particles flow velocity equal to 10^{-6} m/s and practically negligible small average acceleration. It is indicated as time instant t_1 required for interrupting of filling. It depends on the friction coefficient value. Hereby, the end the filling is defined as $t_1=10$ s for the frictionless material ($\mu = 0$) and $t_1 = 6.59$ s for frictional ($\mu = 0.3$) and $t_1 = 6.09$ s for highly frictional materials ($\mu = 0.6$), respectively.

Consequently, all dynamical parameters of particles obtained at the end of the filling process are assumed to be the initial conditions for simulation of the discharge process, while a new time scale referred to initial discharge time $t = 0$ is employed for the sake of similarity

4. Microscopic analysis

Application of the DEM to simulation of granular flow opens new vistas to highlight the microscopic nature of granular material phenomenon in hand. In the framework of current approach, microscopic analysis comprises investigation of a time-evolution of the mean coordination number of the particulate material during filling, variation of the inter-particle contact forces within granular material and the analysis of the particles velocity fields.

The coordination number is the number of contacts for a given particle. It represents microscopic parameter of the granular material which has been widely used for characterization of homogeneity of granular structure. Its mean value characterizes an assembly of particles and is computed as the sum of all particle contacts divided by the number of particles. The time evolution of this state variable during filling is plotted in Fig. 2.

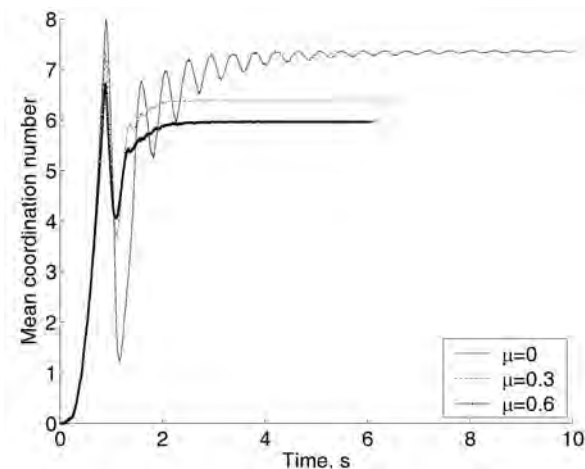


FIG. 2. Time evolution of the mean coordination number of the material during filling.

As it can be seen in Fig. 2, the higher values of coordination number are obtained for frictionless material, while for frictional media, this number decreases with increasing of the particle friction coefficient. The values of the mean coordination number fluctuate in time, and it should be noted that these fluctuations have similarity with the total kinetic energy of particles.

The time evolution of the mean coordination number of the particle may be conditionally distinguished in three stages. The initial stage indicates densification phase. It illustrates that the particles gradually come into contact each with other, transforming from the contactless particles settling indicated by the “zero” coordination number, up the maximal number indicating contact with the hopper’s bottom. It can be clearly seen in the graph (Fig. 2), where at time in-

stant 1 s the material is characterized by the maximal value of the coordination number, varying in the range between 6.5 and 8, depending on the inter-particle friction coefficient.

The second stage indicates rarefaction phase. By passing a very short period of the contact, the particles rebound from the bottom leading to a drastic material rarefying and decrease of the mean coordination number of particles. In particular, for frictionless particles, this reduction is up to 1.5 while the frictional assemblies are less sensitive to this loosening of the packing (coordination number is of about 4), since the particles additionally dissipate their energy due to friction and undergo the confined motion.

Starting from 2–3 s, the evolution of the mean coordination number of particle transforms into the stage of stabilization which is characterized by the values equal to 7.34, 6.38, 5.96 for $\mu = 0$, $\mu = 0.3$, $\mu = 0.6$, respectively, remaining almost constant until the end of the filling. Actually, the results obtained depend on the hopper parameters and filling scenario; however, the peculiarly lower connectivity of the granular structure formed by frictional particles can be attributed to the formation of small arches within the material. It is noticeable that the maximal values of the mean coordination number of particles obtained before the first material rarefying (due to contact with the bottom) cannot later reach the prior maximal value until the end of the filling process.

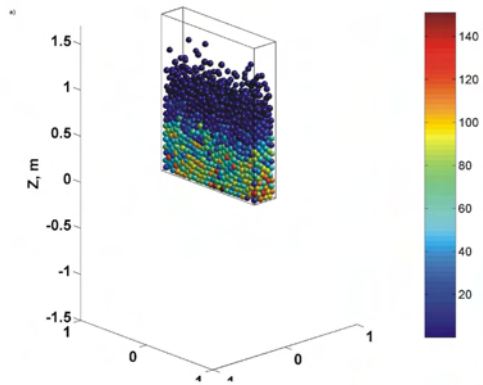
The microscopic state of the particles may be defined by the contact forces acting on the individual particles, while capturing the values of these forces render the quantitative information about the nature of granular structure. In other case, the analysis of contact force network provides the qualitative information about the heterogeneity of granular structure. Consequently, following this concept, let us consider the contact force distribution obtained during the filling and discharge periods.

The character of filling and discharge, indicating the transitional and final stages of the flow in hoppers, is illustrated in Figs. 3 and 4. The colour-bar plotted in these figures quantitatively represents the particle contact forces, $\sum_{i \neq j} |\mathbf{F}_{ij}|$.

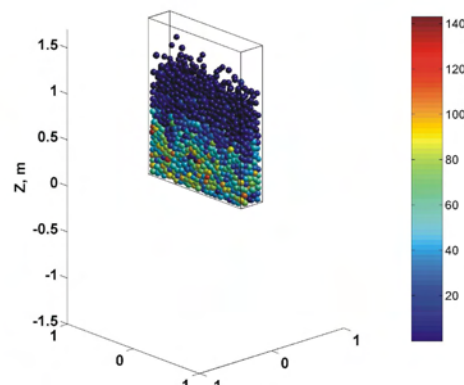
The transitional and the final stages for frictionless ($\mu = 0$) and frictionally rough ($\mu = 0.6$) material clearly exhibit granular material flow during the filling process (Fig. 3). It is easy to indicate forming of the material layers having different contact force transmission within the hopper. In the upper layers of granular structure these forces are distributed more uniformly, while the layers above the bottom are characterized by non-uniformly distributed contact forces. The magnitudes of contact forces at the top surface are much lower as compared to those at the bottom layer, since they grow along the direction of gravity force. Comparing the transitional and final stages, it can be seen that the particle

acceleration during the filling flow affects the magnitudes of particle contact forces. In particular, the maximal value of these forces in transitional state is to a higher than in the final stage. In transitional state, it can also be seen that frictionless particles are subjected a higher maximal contact force of magnitude equal to 155 N as compared to frictional forces (140 N), since the latter dissipate additional portion of kinetic energy during frictional contacts. As it can also be seen, the particle friction produces an increase of the local heterogeneity of the particle contact force transmission, which is higher for rough particles ($\mu = 0.6$) than for smooth ones ($\mu = 0$). It can also be demonstrated that there are some rough particles subjected to much higher contact forces, in comparison with the smooth ones in the lower part of the hopper. It is also seen that due to arching, rough particles located at the vertical wall (Fig. 3, d) form unfilled voids unlike the frictionless particles (Fig. 3, c).

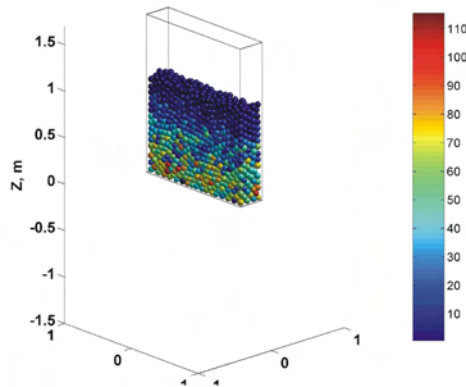
a) $\mu = 0$



b) $\mu = 0.6$



c) $\mu = 0$



d) $\mu = 0.6$

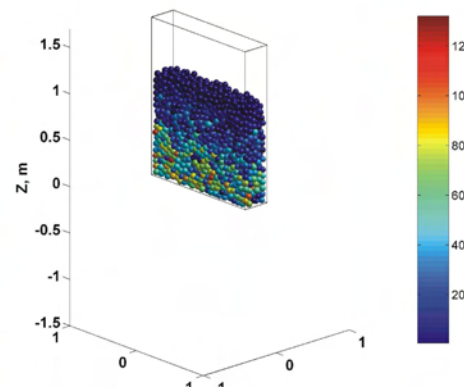


FIG. 3. Filling flow and contact forces (measured in newtons): a, b) transitional ($t = 1$ s); c, d) final stages.

In general, the discharge process in flat-bottomed hopper starts with progressing dilation wave which spreads up to the top surface of the material. The depression zone above the orifice occurs at some material height and deepens with continuation of the discharge process. Its sides become steeper and when the slope of these sides reaches the angle of repose, some of the particles cascade down to the central part of the material which moves faster. The nature of granular flow in the flat-bottomed hopper contains characteristic features of a funnel flow. For brevity, the transitional stages of the discharging flow for frictionless ($\mu = 0$) and for rough ($\mu = 0.6$) particles are captured at time instance $t = 0.2$ s as depicted in Fig. 4. These plots demonstrate the mentioned tendencies about the local heterogeneity of the particle contact force transmission within a granular material. It is also indicated that there are much more rough particles subjected to higher contact forces in comparison with the smooth ones. A common feature of the discharge in the flat-bottomed hopper can be observed, namely the particles located above the orifice up to the top surface of material are practically unloaded when the orifice is opened. On the contrary, for particles located at corners of the hopper walls (stagnant material zones) the contact forces remain almost unchanged during the discharge period. These particles are compressed by the material flowing from above.

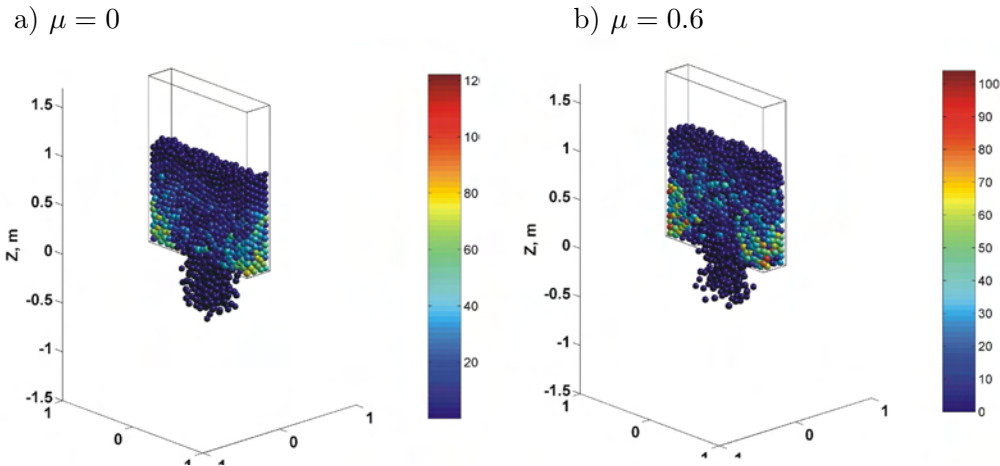


FIG. 4. Discharge flow and contact forces at time instance $t = 0.2$ s (forces measured in newtons).

The significant information about the particle connectivity and contact forces can be obtained by considering the particle contact forces network. Figure 5 and 6 show such a network which is represented by lines connecting the contacting

particles. Thickness of these lines is scaled proportionally to the force magnitude which is fixed by the magnitude of the maximum contact force, hence only qualitative comparison between the networks can be obtained.

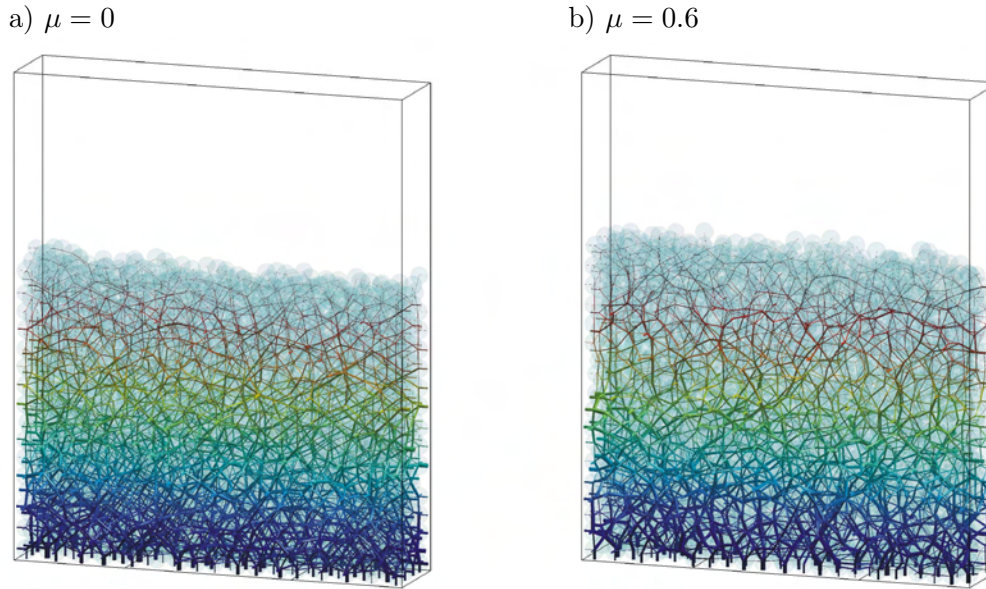
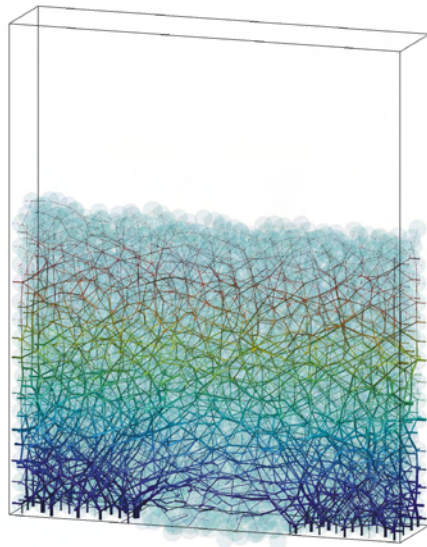
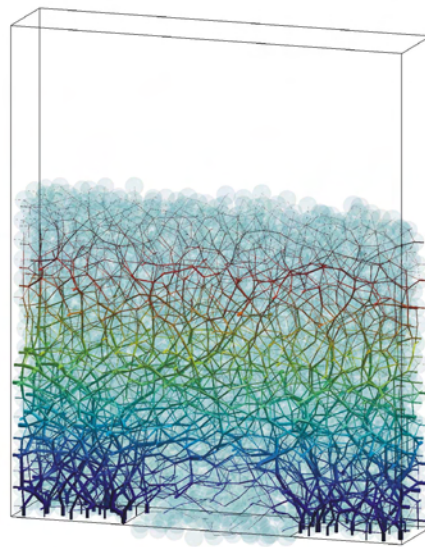
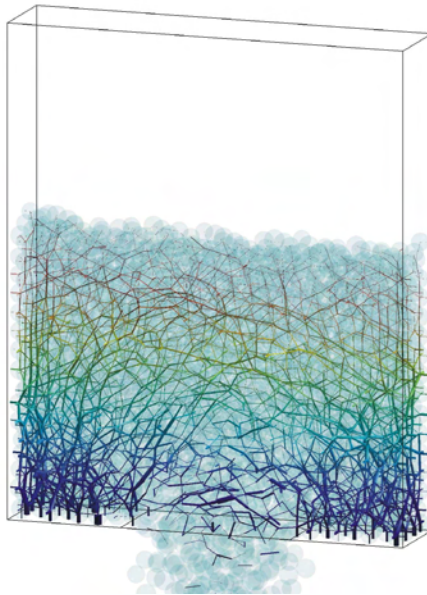
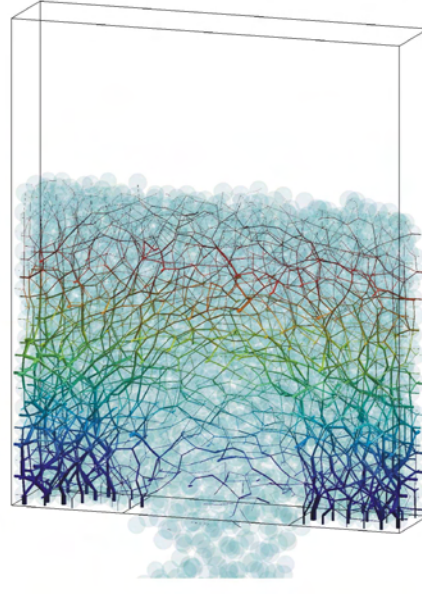


FIG. 5. Contact forces network at the end of filling.

As the graphs in Fig. 3 and the plots in Fig. 5 show, the particle contact forces grow along the gravity force. For frictionless particles, the contact force magnitude network is quite uniform and isotropic within the material depth as well as over all particle contacts. The particle friction induces an increase of local heterogeneity in contact force transmission. Frictional contacts provide a lower connectivity; however, large contact forces can be observed by particles located in lower part of the material and close to the walls. Large contact forces are able to form stress arches leading to the material weight transmission towards the hopper's walls. The experimental demonstrations of such force network can be found in [43].

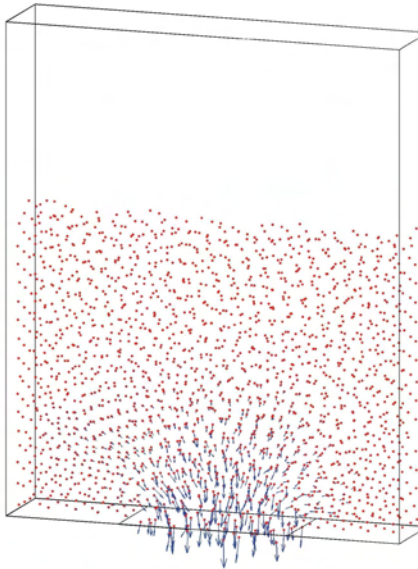
The spatial contact force evolution within material during the discharge is plotted in Fig. 6. It can be indicated that large forces are experienced by particles located at the walls around the bottom corner. Particles located in the upper part have smaller contact forces. Small forces are also found by particles located in a region of a “free-fall arch” which is adjacent to the orifice where particles can accelerate almost freely.

a) $\mu = 0$ b) $\mu = 0.6$ c) $\mu = 0$ d) $\mu = 0.6$ FIG. 6. Contact forces network during discharge at : a, b) $t = 0.04$ s; c, d) $t = 0.2$ s.

From plots depicted in Figs. 6b, d it can be evidently seen that the height of “free-fall arch” region at the initiation of the discharge ($t = 0.04$ s) is of the order of $1/2$ of the orifice width, D (see Fig. 1), while later (when flow becomes steady) it remains constant and approximately equal to D . Above this region the particles are packed together confining each other’s motion, while below it can be seen that particles fall almost without contacts. In the case of frictionless particles (Fig. 6a,c), it can be demonstrated that the region of “free-fall arch” does not exist and particles outflow depends on the material height.

Let us consider the discharge flow kinematics. The distribution of velocity fields has been extensively studied by the macroscopic experiments and simulations, cf. e.g. [10], [28]. However, the detailed motion of individual particles in the discharge flow is difficult to measure experimentally, particularly in the case of 3D. Thus, following the classical macroscopic description of the discharge flow, there are five zones of flow inside the flat-bottomed hopper: stagnant zones located at the bottom corners, a plug flow zone in the upper part, a converging flow zone in the lower part, a transition zone from plug flow to converging flow (where particles move toward the orifice), and a free particle fall zone. From the initial transient stage ($t = 0.04$ s) up to the pseudo-steady ($t = 0.4$ s) flow, such flow patterns can be observed by the obtained velocity vectors of individual particles plotted in Fig. 7.

a) $\mu = 0$



b) $\mu = 0.6$

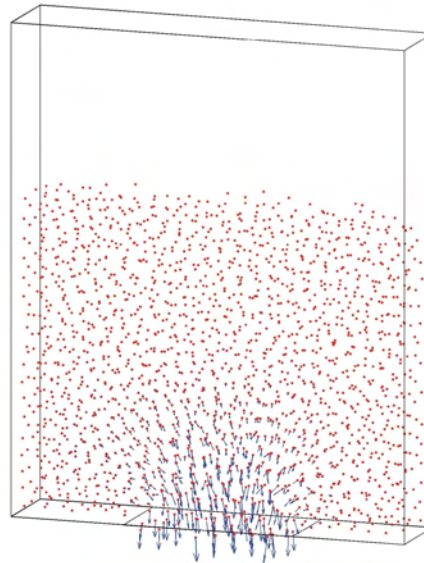


[FIG. 7a, b]

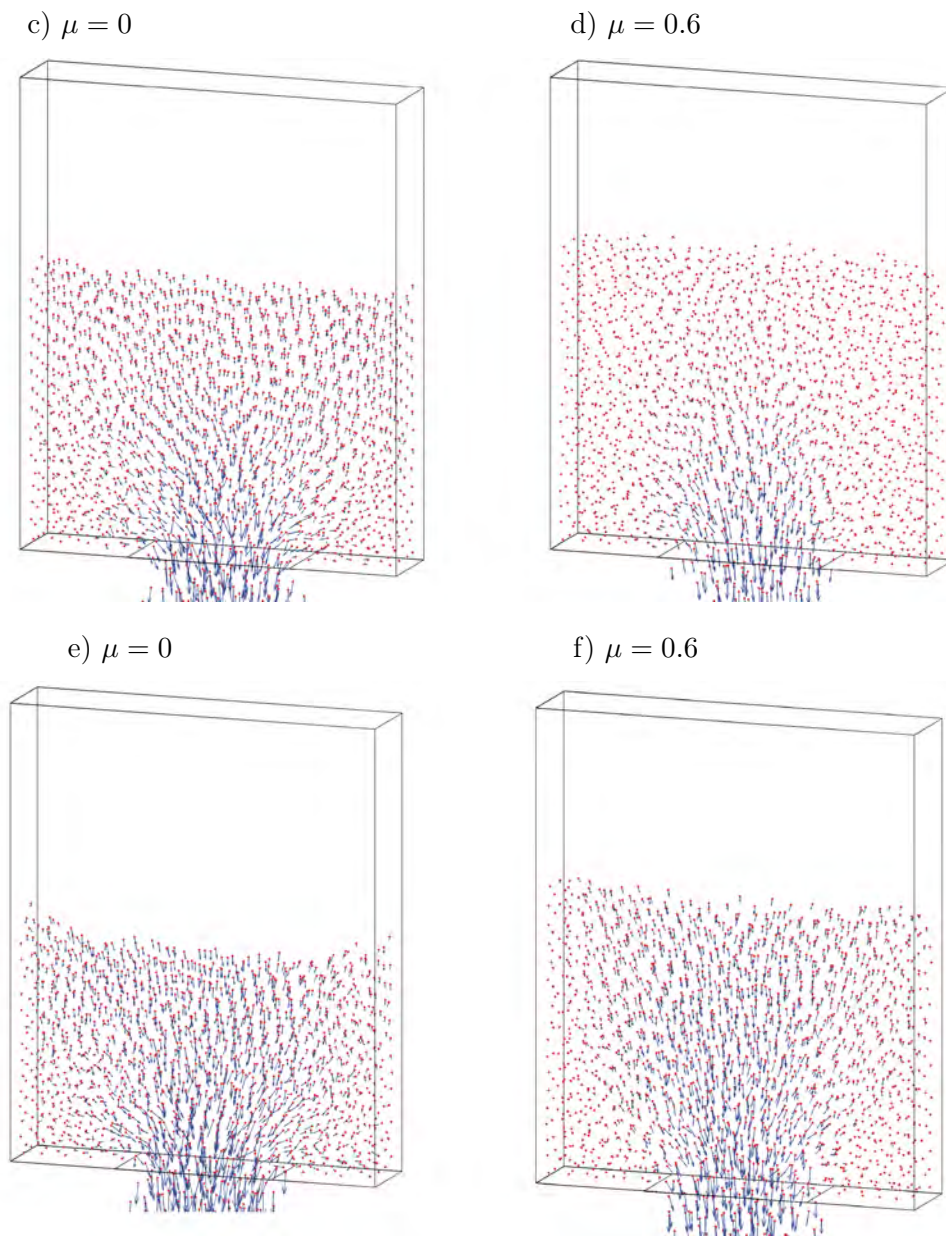


FIG. 7. Contact forces network during discharge at: a, b) $t = 0.04$ s; c, d) $t = 0.2$ s; e, f) $t = 0.4$ s.

The initial transient stage of the discharge runs in the same manner for frictionless and frictional particles (Figs. 7a, b), however the latter flow proceeds

quite differently. Particularly, in Figs. 7e, f it is seen that the converging flow zone is enclosed on both sides by stagnant zone of material with “zero” particle velocities. Stagnant zones form two flow converging boundaries whose shape changes during the discharge. The inclination of these boundaries depends on the particle and wall friction. It is seen that the frictionless particles have a less sharp flow convergence than particles with friction contacts (Figs. 7e, f). It is also observed that a plug flow zone in the case of frictionless particles runs almost vertically and can rather be treated as a mass flow zone (Figs. 7c, e).

5. Macroscopic analysis

The simulation is also utilized to calculate the normal and shear stresses acting on the hopper walls. The values of the wall stresses at different heights are obtained by averaging over the height equal approximately to four particle diameters. The results obtained are compared with the well-known Janssen’s analytical solution [8] which, with certain corrections [10], is used in most standards for predicting the filling pressures in flat-bottomed sections of hoppers. The identification of Janssen’s macroscopic parameters from the simulation corresponds to the bulk density values equal to 335, 325 and 320 kg/m³ for cases of $\mu = 0$, $\mu = 0.3$ and $\mu = 0.6$, respectively. The internal friction angle, ϕ , following [44], is determined by the angle of stagnant boundary zone assumed to be an internal slip plane. By the additional examination of particles funnel-flow fields, values of $\phi = 6 \div 12^\circ$ are obtained. The pressure fields obtained at the end of the filling hopper wall and Janssen’s macroscopic prediction are shown Fig. 8a.

Despite the quite small number of particles used in simulation, the obtained pressure dependence on material height is quite consistent with macroscopic prediction. As it can be seen in Figure 8a, the increased values of the friction coefficient results in a transition from fluid-like to granular material behavior.

The pressure distribution captured during discharge is plotted in Fig. 8 b. As it can be seen, the wall pressure during discharge is lower than at the end of filling. This result contradicts a well-known experimental fact that upon opening of the orifice in a large silo, the wall pressure significantly increases in comparison with the pressure observed at the end of filling. This increase is always very remarkable in the wedge-shaped hopper, where due to the converging flow towards the orifice, the passive stress state can develop, while in the flat-bottomed hopper this increase is lower and mainly depends on the hopper geometry and the angle of stagnant zone resulting in the converging flow. In our case, the drop in lateral wall pressure during discharge is mainly attributed to a relatively large size of orifice and a squat shape of hopper, resulting in a quick reduction of material weight as well as its dilation upon orifice opening. The propagation of material dilation is studied below.

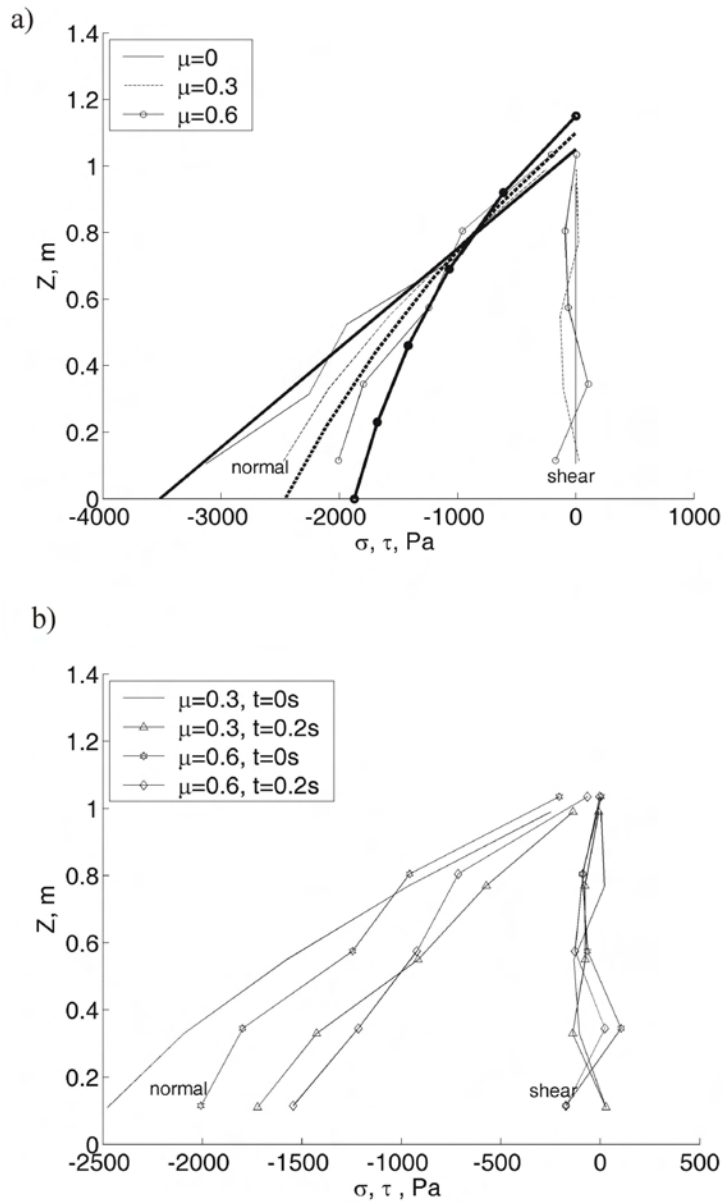


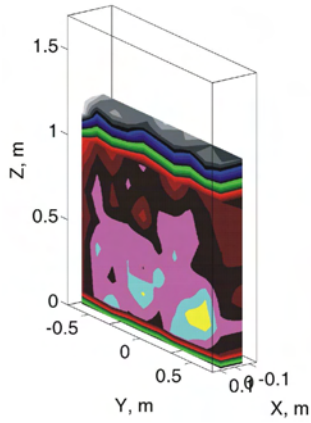
FIG. 8. Evolution of wall pressure at the end of fill a) and during the discharge b). Bold line – Janssen's prediction.

Thus, the macroscopic variable, such as the bulk porosity, reflecting the packing structure of the material within the hopper and directly affecting the bulk

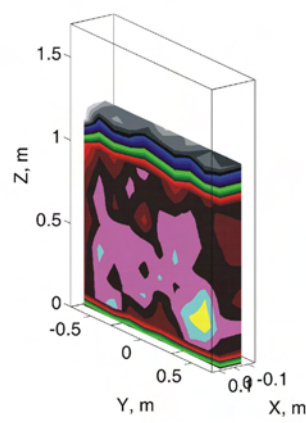
density, can be considered in terms of the spatial distribution of the porosity fields within the granular material. The porosity is specified by averaging of particles volume within the chosen elementary volumes represented by spheres. The volume of the granular structure computed within the representative sphere is defined by excluding the overlaps of the particles. The volume of the representative sphere adjacent to the wall is also defined relying on the sphere-wall intersection geometry. Finally, the computed volumetric data of the porosity are displayed on a spatial grid (Fig. 9).

In general, it has been well-established that the coordination number decreases with the porosity. Such correlation can be easily kept to track within the whole period of the material packing history plotted in Fig. 2. For brevity,

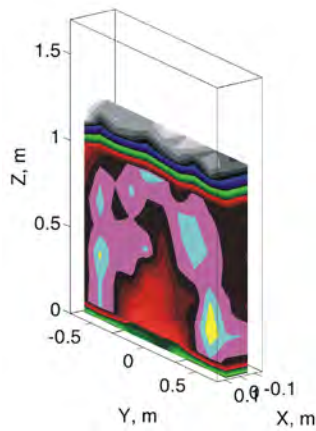
a) $t = 0$ s



b) $t = 0.04$ s



c) $t = 0.2$ s



d) $t = 0.4$ s

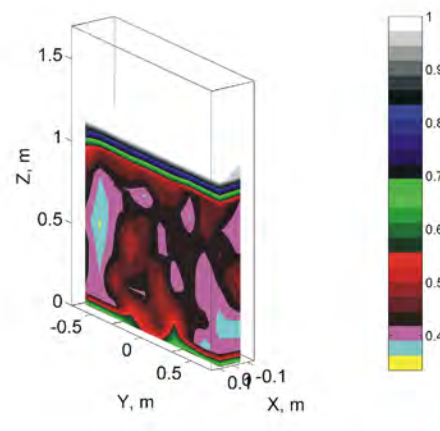


FIG. 9. Time evolution of the porosity fields during discharge ($\mu = 0.6$).

the spatial evolution of the porosity within the hopper is restricted here for the frictionless particles with $\mu = 0.6$ (Fig. 9).

The obtained spatial distribution of the porosity at the end of filling is shown in Fig. 9a. Independently of the roughness of the particle, formation of the densest assemblies is characterized by the lowest values of the porosity which is observed in the lower part of the hopper, while the loose granular structures are located in the upper part, near the walls and in the narrow boundary layer above the bottom. Thus, in the case of frictionless granular material ($\mu = 0$), the dominating porosity values are $n = 0.27 \div 0.3$, while for $\mu = 0.3$ and for $\mu = 0.6$ these values are $n = 0.29 \div 0.32$ and $n = 0.33 \div 0.36$, respectively. The depth of the dominating porosity zones is spread up to the elevation of $0.7 \div 0.9$ m.

The captured evolution of the porosity fields (Figs. 9 b–d) within the hopper clearly exhibits the well-known phenomenon that the orifice opening generates a dilation of the bulk material. At the short time instance after orifice opening ($t = 0.04$ s), the zone of material rarefying with porosity $n = 0.39 \div 0.42$ begins to form in vicinity of the outlet (Fig. 9b). At time instance $t = 0.2$ s this porosity wave reaches in about 0.8 m of the material height, while the dilation above the orifice increases up to the porosity values $n = 0.5 \div 0.53$ (Fig. 9c). Later (at $t = 0.4$ s), each zone of material up to the top of the filling is reached by this dilatancy wave (Fig. 9d).

In addition, by considering the plots shown in Figs. 9 b–d and Figs. 7 b,d,e, it is simple to note that high porosity corresponds to high velocities of the particle.

Let us examine the discharge flow rate (i.e. mass discharged flux) through the orifice. By generalization of numerous empirical observations of the granular flow [10], the main conditions defining a constant discharge rate, when the rate is effectively independent of the quantity of material in hopper characterized by material height z , have been established: $z > 2D$ and $L > 2.5D$. Actually, these conditions highlight the fact about the sufficient material quantity within the hopper which allows to obtain a constant flow rate in time. Hence, for appropriate z and L , the rate depends only on the bulk density, the orifice diameter, gravity acceleration and the material friction. Oppositely, for inviscid liquid the discharge flow rate is proportional to $D^2 \sqrt{2gz}$ (where g is the gravity acceleration). For a rectangular orifice, the discharge rate can be calculated by the following relation [10]:

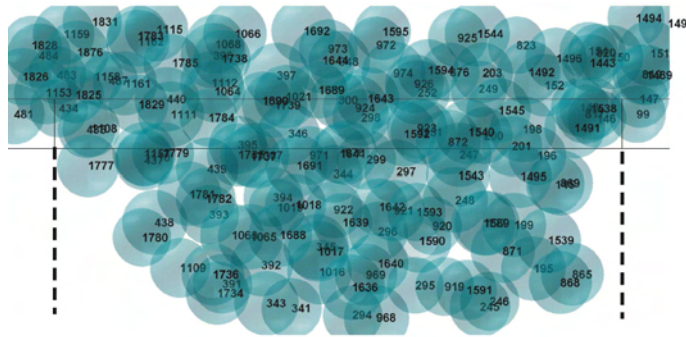
$$(5.1) \quad \frac{dm}{dt} = \frac{8C}{\pi\sqrt{2}} \rho^* \sqrt{g} \frac{((D - kd)(b - kd))^{3/2}}{(D + b - 2kd)^{1/2}}$$

where ρ^* is the bulk density near the orifice, kd is the width of the so-called “empty annulus”, C is the material constant which, following [10] is assumed to be 0.64 for exceptionally smooth spherical particles and 0.58 for the rough ones.

The empirical factor k must be determined experimentally and is claimed to be derived from the concept of the obstruction surrounding region near the orifice generating the flowing particle interaction. This is consistent with the concept of an “empty annulus” proposed by BROWN and RICHARDS [45]. Values of k may vary in a broad range, in particular, from 0.94 for the glass bed [46] up to 4 for sand [47].

However, the region near the orifice surround obstructing the passage of particles is difficult to be observed experimentally. It can simply be defined visually by observing time evolution of particle flow trough the orifice, captured in Fig. 10. It is seen that less particles can be detected close to the orifice corners than in the central region, clearly confirming the concept of “empty annulus”. This effect is also familiar as “vena contracta” meaning the reduced size of the effective flow area with respect to the geometrically specified area. The effect of “vena contracta” is clearly seen in Fig. 10. In particular, it can be seen that kd changes from zero to grain diameter (Fig. 10a), over the range of $0.5 \div 1$ (Fig. 10b, d) by about 2 (near #825 particle in Fig. 10c). Hence, it is reasonable to assume $k = 0.75$.

a) $t = 0.2, \mu = 0.3$



b) $t = 0.2 \text{ s}, \mu = 0.6$

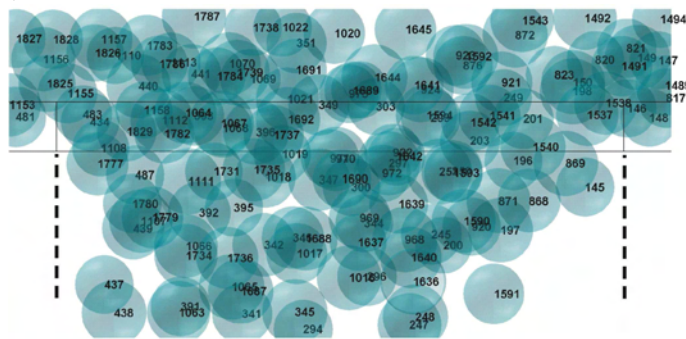


[FIG. 10a, b]

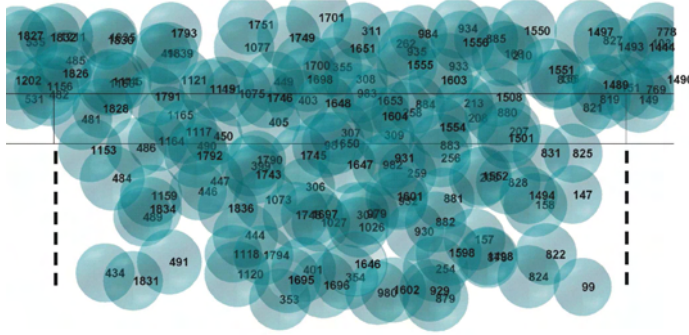
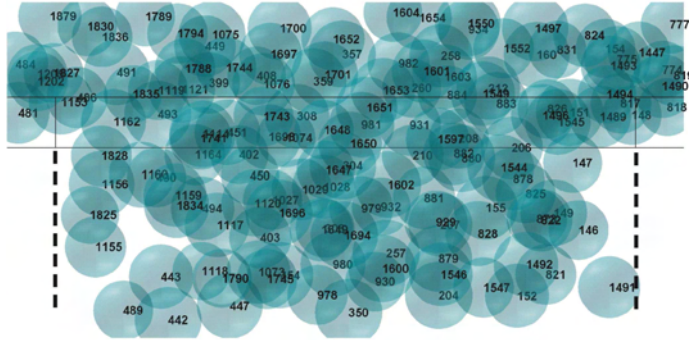
c) $t = 0.4$ s, $\mu = 0.3$ d) $t = 0.4$ s, $\mu = 0.6$ 

FIG. 10. Time evolution of particles flow through the orifice.

Thus, the material flow rate is measured in the discharge simulation and is compared with the theoretical prediction specified by Eq. (3.4) (see Fig. 11). The bulk density near the orifice is derived by the averaged porosity (Fig. 9) within the “free-fall arch” region with its height equal to D . In particular, it has the values of 295, 270 and 260 kg/m³, for cases of $\mu = 0$, $\mu = 0.3$ and $\mu = 0.6$, respectively. These values indicate approximately 13÷23% reduction of the bulk material density packed at the end of the filling.

As it can be seen in Fig. 11, the current simulation indicates the empirical evidence that for the increasing particle friction coefficient, the rate of discharge is reduced. It is seen that this reduction represents a mild function of the particle friction coefficient and is adequate to the experimental observations. For frictionless particles ($\mu = 0$), an expected nonlinear variation of mass discharged flux is observed. For frictional particles, the discharge rate exhibits some fluctuations in time however, in the case of $\mu = 0.6$ the constant rate can be observed in the time period from 0.2 s to 1 s.

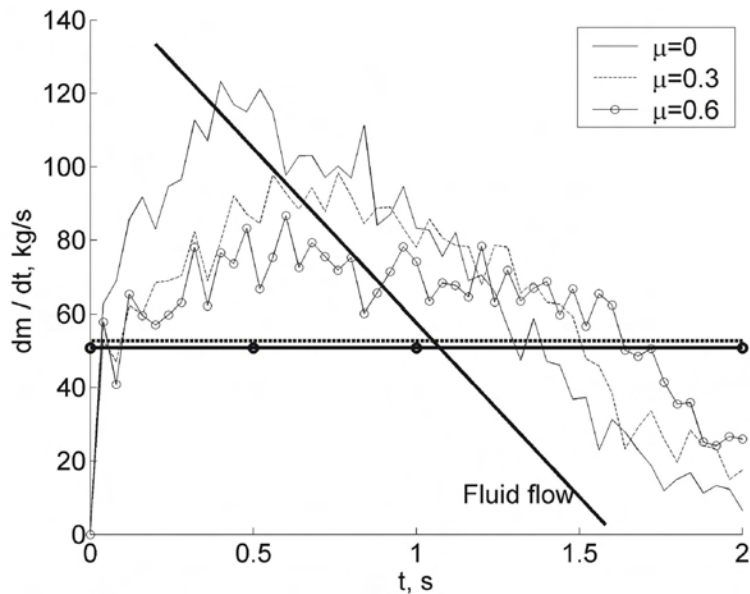


FIG. 11. Evolution of the discharge rate. Bold line – macroscopic prediction by (5.1).

The agreement between the prediction based on Eq. (5.1) and the results of the simulation would be closer, if the particle sizes were smaller resulting in a much greater number of particles and a closer approach to the continuum. Furthermore, the variation of the discharge flow rate in time is generally attributed to small height of the hopper. In such case, the material resupply into the hopper during discharge allows to obtain more steady discharge flow with fewer fluctuations [28].

6. Concluding remarks

Filling and discharge processes of the granular material in a flat-bottomed rough-walled hopper are simulated by the three-dimensional discrete element model. The model is based on a single particle contact mechanics constitutive laws with Hooke's spring interaction, static and dynamic frictions as well as viscous damping forces. The main focus of the paper was a qualitative illustration of the physical processes inside the time-dependent flow of granular material and the consistency of micro and macro descriptions.

Generally, despite the small number of particles in the current analysis, the consistency of micro and macro-descriptions has been proved. The micromechanical aspect of the macroscopically observable phenomenon is additionally exhibited by introducing the microscopic variables, such as coordination num-

ber, inter-particle contact forces or particle displacements and velocities defined at the particle scale. The analysis performed has shown that particle friction has a major influence on the material flow kinematics, the changes in porosity and stress fields. On the basis of numerical simulation, the following conclusions may be summarized as follows:

- The consistency between the obtained wall pressure and its macroscopic equivalent based on Janssen's formula was found by considering the end of filling stage for frictional and frictionless particles. In the discharge, the obtained drop in pressure was affected due to squat shape of hopper and relatively large orifice inducing a sudden reduction of the material weight.
- Evolution of material packing during filling illustrates that the final quasi-static state in the hopper is characterized by the lower coordination number as compared to the highest value reached by the first densification wave. Such aspect is relevant to the particle viscous damping/elasticity balance and filling scenario, ensuring a close packing structure during particle settling in the hopper.
- The obtained spatial distribution of bulk porosity within a granular material has demonstrated the fact about the propagation of the experimentally observed dilation wave occurring after opening of the orifice. During a short period this wave reaches the top material, surface and occupies almost the whole material causing the decompression of particle contact forces, which in turn leads to the reduction of wall stresses.
- Microscopic motion of particles during the discharge illustrated by the velocity profiles corresponds qualitatively to macroscopic profiles experimentally observed in real funnel-flow hoppers. Time evolution of bulk porosity and the individual particle velocities simply demonstrate the fact that high porosity corresponds to high particle velocity.
- The obtained spatial distribution of the particle contact forces within the flowing frictional particles demonstrated a decisive role of the inter-particle friction and exhibited fundamental differences between frictionless and frictional granular matter by characterization of the so-called "free-fall arch" region.
- The concept of the so-called "empty annulus" or "vena contracta" and a mild influence of particle friction on discharged mass flow rate have also been highlighted in the current analysis. The existing predictions of the steady-state discharged mass flow rate of the frictional material present slightly lower bounds of the numerically simulated evaluations.

The results presented are considered as a preliminary investigation of real grain materials. For more accurate simulation, the aggregate of larger number of grains should be analyzed with a realistic grain size distribution function. This will constitute a subject of future studies.

Acknowledgments

The fourth author expresses her deep gratitude for the financial support of the Rector Project W/IIB/11/06.

References

1. H. M. JAEGER, S. R. NAGEL, R. P. BEHRINGER, *Granular solids, liquids, and gases*, Reviews of Modern Physics, **68**, 4, 1259–1273, 1996.
2. J. M. HUNTLEY, *Fluidization, segregation and stress propagation in granular materials*, Philosophical Transactions of the Royal Society A: Mathematical, Physical and Engineering Sciences, **356**, 2569–2590, 1998.
3. P. G. DE GENNES, *Granular matter: a tentative view*, Reviews of Modern Physics, **71**, 2, S374–S382, 1999.
4. H. J. HERRMANN, *Granular matter*, Physica A, **313**, 188–210, 2002.
5. S. C. MCNAMARA, H. J. HERRMANN, *Quasirigidity: Some uniqueness issues*, Physical review, E **74**, 061303-1–061303-14, 2006.
6. A. W. ROBERTS, *Particle and bulk solids handling technology – bridging the theory practice gap*, Fifth World Congress on Particle Technology April 23–27, 2006, Orlando, Florida, USA, CD ROM proceedings, 1–38, 2006.
7. A. W. ROBERTS, *Characterization of hopper and stockpile design*, In Characterization of bulk solids, D. McGLINCHEY [Ed.], Blackwell Publishing, 85–131, 2005.
8. H. A. JANSSEN, *Versuche über Getreidedruck in Silozellen*, Z. Ver. Dt. Ing., **39**, 1045–1049, 1895.
9. A. DRESCHER, ANALYTICAL METHODS IN BIN-LOAD ANALYSIS, Elsevier, Amsterdam-Oxford-New York-Tokyo 1991.
10. R. M. NEDDERMAN, *Statics and kinematics of granular materials*, Cambridge University Press, New York 1992.
11. Z. Mróz, Cz. Szymański, *Gravity flow of granular material in a converging channel*, Arch. Mech., **23**, 897–917, 1971.
12. Z. MRÓZ, I. SIELAMOWICZ, *Deformation zones in granular materials in converging hoppers during filling and emptying processes*, Engineering Transactions, **51**, 4, 461–491, 2003.
13. D. O. KRIMER, M. PFITZNER, K. BRÄUER, Y. JIANG, M. LIU, *Granular elasticity: General considerations and the stress dip in sand piles*, Physical review E, **74**, 061302-1–061310-10, 2006.
14. K. BRÄUER, M. PFITZNER, D. O. KRIMER, M. MAYER, Y. JIANG, M. LIU, *Granular elasticity: Stress distributions in silos and under point loads*, Physical review E, **74**, 06061311-1–061311-10, 2006.
15. J.W. LANDRY, G.S. GREST, S.J. PLIMPTON, *Discrete element simulations of stress distributions in silos: crossover from two to three dimensions*, Powder technology, **139**, 233-239, 2003.

16. M. SPERL, *Experiments on corn pressure in silo cells-translation and comment of Janssen's paper from 1985*, *Granular Matter*, **8**, 59–65, 2006.
17. J.M.F.G. HOLST, J.Y. OOI, J.M. ROTTER, G.H. RONG, *Numerical modeling of silo filling: I. Continuum analyses*, *J. Eng. Mech.*, **125**, 94–103, 1999.
18. J. TEJCHMAN, G. GUDEHUS, *Silo-music and silo-quake experiments and a numerical Cosserat approach*, *Powder Technology*, **76**, 2, 201–212, 1993.
19. S. A. ELASKAR, L. A. GODOY, D. D. GRAY, J. M. STILES, *A viscoplastic approach to model the flow of granular solids*, *International Journal of Solids and Structures*, **37**, 2185–2214, 2000.
20. J. TEJCHMAN, T. UMMENHOFER, *Bedding effects in bulk solids in silos: experiments and a polar hypoplastic approach*, *Thin-Walled Structures*, **37**, 333–361, 2000.
21. P. A. CUNDALL, O. D. L. STRACK, *A discrete numerical model for granular assemblies*, *Geotechnique*, **29**, 47–65, 1979.
22. A. DŽIUGYS, B. J. PETERS, *An Approach to Simulate the Motion of Spherical and Non-Spherical Fuel Particles in Combustion Chambers*, *Granular Material*, **3**, 4, 231–266, 2001.
23. P. W. CLEARLY, M. L. SAWLEY, *DEM modelling of industrial granular flows: 3D case studies and the effect of particle shape on hopper discharge*, *Applied Mathematical Modelling*, **26**, 89–111, 2002.
24. C. S. CAMPBELL, C. E. BRENNEN, *Computer simulation of shear flows of granular material. Mechanics of granular materials: New models and constitutive relations* [in:], J. T. JENKINS and M. SATAKE [Eds.], Elsevier, Amsterdam 1983.
25. O. R. WALTON, *Particle –dynamic calculations of shear flow. Mechanics of granular materials: New models and constitutive relations*, J. T. JENKINS and M. SATAKE [Eds.], Elsevier, Amsterdam 327–338, 1983.
26. C. THORNTON, *APPLICATION OF DEM TO PROCESS ENGINEERING PROBLEMS IN DEM*, [in:] 1-st US Conference, Colorado School of Mines Press, 87–100, 1989.
27. S. MASSON, J. MARTINEZ, *Effect of particle mechanical properties on silo flow and stresses from distinct element simulations*, *Powder Technology*, **109**, 164–178, 2000.
28. P. A. LANGSTON, U. TÜZÜN, D. M. HEYES, *Continuous potential discrete particle simulations of stress and velocity fields in hoppers. Transition from fluid to granular flow*, *Chemical Engineering Science*, **49**, 8, 1259–1275, 1994.
29. H. P. ZHU, A. B. YU, *Steady-state granular flow in 3D cylindrical hopper with flat bottom: macroscopic analysis*, *Granular Matter*, **7**, 97–107, 2005.
30. J. F. FERELLEC, J. MARTINEZ, S. MASSON, K. IWASHITA, *Influence of particle rolling resistance on silo flow in DEM simulations*, [in:], KISHINO [Ed.], *Powders and Grains*, Swets and Zetlinger, Lisse, 409–412, 2001.
31. D. HIRSHFELD, D. C. RAPAPORT, *Granular flow from a silo: discrete-particle simulations in three dimensions*, *Eur. Phys. J. E*, **4**, 193–199, 2001.
32. R. BALEVIČIUS, R. KAČIANAUSKAS, Z. MRÓZ, I. SIELAMOWICZ, *Discrete Element Method applied to multiobjective optimization of discharge flow parameters in hoppers*, *Structural and Multidisciplinary Optimization*, **31**, 3, 163–175, 2006.

33. P. A. LANGSTON, M. A. AL-AWAMLEH, F. Y. FRAIGE, B. N. ASMAR, *Distinct element modeling of non-spherical frictionless particle flow*, Chemical Engineering Science, **59**, 425–435, 2004.
34. J. LI, PA LANGSTON, C. WEBB, T. DYAKOWSKI, *Flow of sphero-disc particles in rectangular hoppers – a DEM and experimental comparison in 3D*, Chemical Engineering Science, **59**, 5917–5929, 2004.
35. J. S. LESZCZYŃSKI, *A discrete model of the dynamics of particle collisions in granular flows*, Monograph no. 106, Częstochowa University of Technology, Częstochowa 2005.
36. J. S. LESZCZYŃSKI, *A discrete model of a two-particle contact applied to cohesive granular materials*, *Granular Matter*, **5**, 2, 91–98, 2003.
37. R. BALEVIČIUS, A. DŽIUGYS, R. KAČIANAUSKAS, *Discrete element method and its application to the analysis of penetration into granular media*, Journal of Civil Engineering and Management, **10**, 1, 3–14, 2004.
38. G. A. KOHRING, *Dynamical simulations of granular flows on multi-processor computers*, Computational methods in applied sciences '96, John Wiley and Sons Ltd., 190–196, 1996.
39. R. D. MINDLIN, H. DERESIEWICZ, *Elastic spheres in contact under varying oblique forces*, J. Appl. Mech. Trans. ASME, **20**, 327–344, 1953.
40. M. P. ALLEN, D. J. TILDESLEY, *Computer simulation of liquids*, Clarendon Press, Oxford, 1991.
41. R. BALEVIČIUS, R. KAČIANAUSKAS, A. DŽIUGYS, A. MAKNICKAS, K. VISLAVIČIUS, *DEMMAT code for numerical simulation of multi-particle dynamics*, Information Technology and Control, **34**, 1, 71–78, 2005.
42. R. BALEVIČIUS, R. KAČIANAUSKAS, A. DŽIUGYS, A. MAKNICKAS, K. VISLAVIČIUS, *Investigation of performance of programming approaches and languages used for numerical simulation of granular material by the discrete element method*, Computer Physics Communications, **175**, 6, 404–415, 2006.
43. O. POULIQUEN, R. GUTFRAIND, *Stress fluctuations and shear zones in quasi-static granular chute flows*, Phys. Rev. E, **53**, 1996, 557–561
44. P. A. LANGSTON, U. TÜZÜN, D. M. HEYES, *Continuous potential discrete particle simulations of stress and velocity fields in hoppers: Transition from fluid to granular flow*, Chemical Engineering Science, **49**, 8, 1259–1275, 1994.
45. R. L. BROWN, J. C. RICHARDS, *Principles of powder mechanics*. Pergamon Press, Oxford 1970.
46. J. CHOI, A. KUDROLLI, M. Z. BAZANT, *Velocity profile of granular flows inside silos and hoppers*, Journal of Physics: Condensed Matter, **17**, S2533–S2548, 2005.
47. T. V. NGUYEN, C. BRENNEN, R. H. SABERSKY, *Gravity flow of granular materials in Conical Hoppers*, Journal of Applied Mechanics, **46**, 10, 529–535.

Received October 4, 2006; revised version April 25, 2007.
